INSTITUTE OF PHYSICS PUBLISHING CLASSICAL AND QUANTUM GRAVITY

Class. Quantum Grav. **21** (2004) S351–S375 PII: S0264-9381(04)70736-4

Time–frequency analysis of the restricted three-body problem: transport and resonance transitions

Luz V Vela-Arevalo[1] **and Jerrold E Marsden**[2]

[1] Center for Nonlinear Science, School of Physics, Georgia Institute of Technology, Atlanta, GA 30332-0430, USA
[2] Control and Dynamical Systems, 107-81, California Institute of Technology, Pasadena, CA 91125, USA

E-mail: luzvela@cns.physics.gatech.edu and marsden@cds.caltech.edu

Received 21 October 2003
Published 13 January 2004
Online at stacks.iop.org/CQG/21/S351 (DOI: 10.1088/0264-9381/21/3/022)

Abstract

A method of time–frequency analysis based on wavelets is applied to the problem of transport between different regions of the solar system, using the model of the circular restricted three-body problem in both the planar and the spatial versions of the problem. The method is based on the extraction of instantaneous frequencies from the wavelet transform of numerical solutions. Time-varying frequencies provide a good diagnostic tool to discern chaotic trajectories from regular ones, and we can identify resonance islands that greatly affect the dynamics. Good accuracy in the calculation of time-varying frequencies allows us to determine resonance trappings of chaotic trajectories and resonance transitions. We show the relation between resonance transitions and transport in different regions of the phase space.

PACS numbers: 95.10.Ce, 02.60.Cb, 05.45−a, 02.30.Uu

Dedicated to Vince Moncrief on the occasion of his 60th birthday.

1. Introduction

Phase space transport in Hamiltonian systems containing both regular and chaotic dynamics is greatly affected by the presence of resonance islands. In fact, chaotic trajectories can be trapped around a resonance for a long time, or can wander around different islands. We show that both the overall phase space structure as well as features of this type of transport can be detected and analysed by the method of time–frequency analysis based on wavelets.

1.1. The goal of this work

We propose the use of a wavelet-based method of time–frequency analysis for the dynamics of Hamiltonian systems in which the trajectories display oscillatory behaviour. This method

was introduced in [1] to study the global dynamics of a molecular system; however, it can be applied in a large variety of systems. Here we extend the scope of the method, and provide a numerical algorithm based on the phase of the continuous wavelet transform (the methodology in [1] uses the modulus of the wavelet transform). Also, this paper presents our application of the method to address the problem of transport and resonance transitions in the solar system using the circular restricted three-body problem (CRTBP).

1.2. Wavelet-based time–frequency analysis

Time–frequency analysis is a numerical tool that allows one to distinguish between regular and chaotic trajectories by computing time-varying frequencies associated with the trajectories. Since quasiperiodic trajectories are characterized by constant frequencies, the time variation of the frequency is a good indicator of chaos.

The method is able to detect resonance islands that greatly affect the dynamics of the system in the sense that they sometimes temporarily 'capture' chaotic trajectories, a dynamical feature observed in asteroids [2] and comets [3]. We can show that chaotic trajectories remaining around a resonance island for some time have frequencies that nearly satisfy the resonance equation during that interval of time. This process is called *resonance trapping*. Since the method we propose yields accurate time-varying frequencies, the technique is able to detect when a chaotic trajectory has been trapped, or has undergone a transition between resonances. The method also reveals how resonance transitions are related to phase space transport.

1.3. The circular restricted three-body problem

The circular restricted three-body problem has been a subject of extensive study in astrodynamics, celestial mechanics and dynamical systems. This is the problem that inspired H Poincaré in his fundamental development of the qualitative theory of dynamical systems and chaos.

The spatial CRTBP is a Hamiltonian system of three degrees of freedom (two in the planar version) describing the motion of a small body attracted by the gravitational forces of two other bodies orbiting in circles around their centre of mass. The model can be applied to systems such as the Sun–Jupiter–comet system, or the Earth–Moon–satellite system; in addition, this model is often used as the starting point in the design of space missions (see, e.g., [4]). The CRTBP has, in general, been an excellent benchmark for testing dynamical systems techniques.

1.4. Application of time–frequency analysis

The main motivation to apply this technique to the CRTBP arises in the context of the results of Koon *et al* [3] that relate the transport mechanism to resonance transitions. In this work, time–frequency analysis is used to study the transport mechanism between the exterior and interior regions with respect to the orbit of a planet in the solar system. In particular, we find that time-varying frequencies associated with orbits in the inertial frame provide enough information to detect transitions between different regions of the phase space. This is why time–frequency analysis is so important for this problem.

A detailed description of the application of the wavelet time–frequency analysis is done for the planar problem; however, we show that the methodology extends naturally to the spatial CRTBP. We show that in the spatial problem the trajectories that undergo transitions between

different regions of the phase space are nearly planar, and we are able to characterize transport in this three-degrees-of-freedom problem.

For the planar problem, Koon *et al* [3] show the existence of homoclinic and heteroclinic connections between periodic orbits around the libration points L_1 and L_2 (the Lyapunov orbits). These connections are obtained as intersections of the invariant manifolds of the Lyapunov orbits. They show that these intersections are in the regions corresponding to the 2:3 and 3:2 resonances. Since the invariant manifolds of the Lyapunov orbits are two-dimensional objects that form tubes in a three-dimensional energy surface, they provide dynamical channels between different regions of the phase space. Therefore, by following the structure of these tubes, Koon *et al* [3] were able to describe an important ingredient in the transport problem of the planar restricted three-body problem. The technique of invariant manifolds has been combined with the method of invariant sets in the work of Dellnitz *et al* [5]; with this approach they have studied transport in the exterior region of the planar CRTBP.

Using time–frequency analysis, we are able to add the time component to the picture given by the invariant manifolds. The method can discern which trajectories undergo a transition between the exterior and interior regions, and we know exactly when this happens; therefore, we can study transport rates in terms of the physical time. With our method, we can detect important resonances that play a role in the transport mechanism. We show that the transport between the exterior and interior regions in the solar system can be explained in large part by transitions between the outer and inner resonances. We also know which trajectories are trapped in the resonances during some period of evolution; therefore, this provides a picture of the system at a given point in time in terms of resonance trappings. We are also able to detect key regions in the phase space in which rapid resonance transitions occur, and compute a rate at which we expect a transition to happen.

An additional advantage over the invariant manifold approach in the study of transport is that time–frequency analysis is applicable in higher dimensions. The computation of invariant manifolds can be extremely difficult, especially for higher dimensional systems and for long-time evolution. Our method provides a good and computationally efficient approach to study transport since by design the method is generalizable to systems of three degrees of freedom or more.

1.5. Other methods

There are several numerical methods available for obtaining qualitative information on dynamical systems, which are based on the treatment of trajectories as time series. Here we discuss briefly the method of Lyapunov exponents, the method of twist angles, and the method of frequency analysis.

The method of Lyapunov exponents [6] is one of the most widely used algorithms for discerning whether a trajectory is chaotic or regular. The method analyses the local displacements between neighbouring trajectories, that reflect on the sign of the largest Lyapunov exponent. If a trajectory is chaotic there is generally an exponential separation between trajectories, and the largest Lyapunov exponent is positive; if the trajectory is regular, then normally the Lyapunov exponent is negative or zero. However, this method usually does not provide additional qualitative information; for example, if a regular trajectory is resonant or non-resonant (quasiperiodic).

The method of twist angles by Contopoulos and Voglis [7, 8] consists of the computation of angles between deviations of the orbit and a fixed direction. This method can differentiate between quasiperiodic and resonant trajectories, but cannot determine the type of resonance

(for instance, a 1:2 resonance corresponds to a trajectory in which the two frequencies involved are in this ratio with respect to each other).

Both the method of Lyapunov exponents and the method of twist angles require the solution of the equations of motion and the first variation equations (the equations corresponding to the linearization of the vector field along trajectories). This additional computational effort can be challenging in systems of large dimension.

The method of frequency analysis by Laskar [9, 10] has been applied extensively for Hamiltonian systems from fields as diverse as galactic dynamics [11], chemical physics [12], celestial mechanics [13] and molecular dynamics [14]. Frequency analysis is based on the windowed Fourier transform (also known as the Gabor transform) for the extraction of frequencies associated with the trajectories. Since the frequencies of regular trajectories remain constant in time, the variation of the frequencies with time provides a good indicator of chaos. The method also allows the identification of resonant motion by analysing the ratios between frequencies.

In this work, we propose a modification of the standard frequency analysis. The introduction of wavelet analysis will allow us to compute instantaneous (or time-varying) frequencies, in a way that is computationally efficient and more generally applicable than the methods based on Fourier analysis. In particular, the treatment of chaotic trajectories is done in a suitable way, since we can detect more efficiently quick variations in frequency. The method of time–frequency analysis based on wavelets presented here allows us to give a detailed description of both chaotic and regular trajectories, and extend the analysis to a description of the transport mechanism in the phase space.

1.6. Organization of the paper

In section 2, we describe the equations of motion and general aspects of the dynamics of the CRTBP. In section 3, we introduce the concept of time-varying frequency and the relevant class of functions for this to be meaningful. In section 4, we describe the method of time–frequency analysis based on wavelets. The application of the method to the CRTBP is described in section 5, and the results of the planar case are presented in section 6. In section 7, we show the main results for the spatial CRTBP, a system of three degrees of freedom. Finally, the conclusions are in section 8.

2. The circular restricted three-body problem

The circular restricted three-body problem is a system in which a small body moves under the attraction of two primary bodies moving in circular orbits in the plane x, y. If the small body is restricted to this plane ($z = 0$), we obtain the planar CRTBP. For instance, the primaries can be the Sun and Jupiter, and the problem will consist of the description of the motion of a comet. The motion of the two primaries is restricted to a particular solution of the Kepler problem: the two bodies move in circular orbits around their centre of mass. The third body is assumed to be small enough so that the motion of the primaries is not influenced by its presence.

When the time and position coordinates are normalized [15], the system has only one parameter μ, which is the ratio between the mass of one primary and the total mass of the system. For instance, for the Sun–Jupiter system with masses m_S and m_J, the mass parameter is

$$\mu = \frac{m_J}{m_J + m_S} = 0.000\,9537.$$

The equations of motion of the third body are given in a rotating frame in the coordinates (x, y), with the same angular velocity as the primaries. In this frame, the primaries are fixed at the points $(-\mu, 0)$ and $(1-\mu, 0)$. The equations of motion can then be expressed as

$$\begin{aligned} \dot{x} &= v_x, \qquad & \dot{v}_x &= 2v_y + x - \frac{(1-\mu)(x+\mu)}{{r_1}^3} - \frac{\mu(x-1+\mu)}{{r_2}^3}, \\ \dot{y} &= v_y, \qquad & \dot{v}_y &= -2v_x + y - \frac{(1-\mu)y}{{r_1}^3} - \frac{\mu y}{{r_2}^3}, \\ \dot{z} &= v_z, \qquad & \dot{v}_z &= -\frac{(1-\mu)z}{{r_1}^3} - \frac{\mu z}{{r_2}^3}, \end{aligned} \tag{1}$$

where ${r_1}^2 = (x+\mu)^2 + y^2 + z^2$ and ${r_2}^2 = (x-1+\mu)^2 + y^2 + z^2$. The equations of motion (1) are the Euler–Lagrange equations corresponding to the Lagrangian function given by

$$L = \frac{1}{2}\big((v_x - y)^2 + (v_y + x)^2 + v_z^2\big) + \frac{1-\mu}{r_1} + \frac{\mu}{r_2} + \frac{\mu(1-\mu)}{2}.$$

The corresponding conserved energy is given by

$$E = \frac{1}{2}\big(v_x^2 + v_y^2 + v_z^2\big) - \left[\frac{1}{2}(x^2+y^2) + \frac{1-\mu}{r_1} + \frac{\mu}{r_2} + \frac{\mu(1-\mu)}{2}\right]. \tag{2}$$

The energy is related to the Jacobi constant C by $E = -C/2$ (see, e.g., [15]).

In this work we are interested in the Sun–Jupiter–comet system for values of the energy close to that of the comet Oterma, $E = -1.515$, that is, Jacobi constant $C = 3.03$ (for a description of the motion of comet Oterma see [3]).

System (1) can also be expressed in Hamiltonian form via the Legendre transformation from the Lagrangian L, with the momenta defined as

$$p_x = v_x - y, \qquad p_y = x + v_y, \qquad p_z = v_z,$$

and the Hamiltonian function given by

$$H = \frac{1}{2}\big[(p_x + y)^2 + (p_y - x)^2 + p_z^2\big] - \frac{1}{2}(x^2+y^2) - \frac{1-\mu}{r_1} - \frac{\mu}{r_2} - \frac{\mu(1-\mu)}{2}.$$

From the equation of conservation of energy (2), one immediately notes that

$$v_x^2 + v_y^2 + v_z^2 = 2E + (x^2+y^2) + 2\frac{1-\mu}{r_1} + 2\frac{\mu}{r_2} + \mu(1-\mu) \geqslant 0.$$

This inequality provides the values of the position coordinates x, y, z for which the motion is allowed; this region is known as the Hill's region. The boundary of the Hill's region is formed by the surfaces (curves in the planar case) for which $v_x = v_y = v_z = 0$ and for a specific value of the energy E.

The Hill's region in the planar case ($z = v_z = 0$) for the Sun–Jupiter system and $E = -1.515$ is displayed in figure 1. Note that the forbidden region (grey) defines three areas where motion is possible: the interior region around the Sun, the Jupiter region and the exterior region.

2.1. Equilibrium points, stability and Lyapunov orbits

The CRTBP has five equilibrium points: the collinear or libration points L_1, L_2 and L_3, and the Lagrangian or equilateral points L_4 and L_5. The values of the energy that we are interested in are slightly higher than the value of the energy at L_2. The corresponding Hill's region for these values divide the phase space into three areas: the interior region around the Sun, the

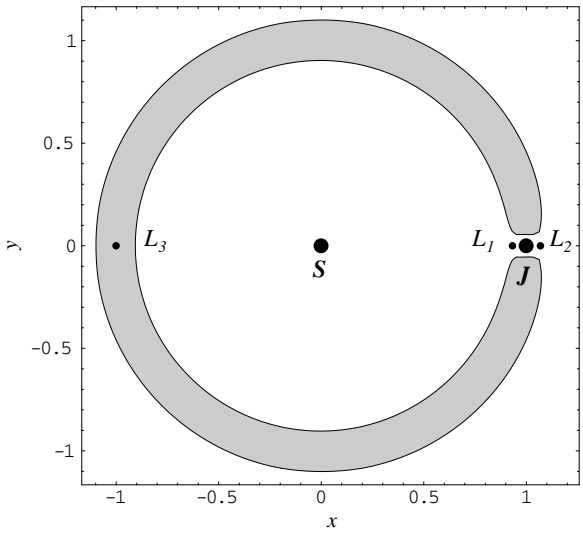

Figure 1. Hill's region of the Sun–Jupiter system ($\mu = 0.000\,9537$). The grey area corresponds to forbidden motion; it divides the configuration space into three regions: the interior region around the Sun, the Jupiter region and the exterior region. The figure corresponds to energy $E = -1.515$, the energy of the comet Oterma.

Jupiter region and the exterior region. The libration points are represented in figure 1; note that the point L_3 is in the forbidden region.

Let us take a closer look at the dynamics in the Jupiter region for the planar case (two degrees of freedom). By studying the linear stability of the libration points L_1 and L_2, it follows that they have one-dimensional stable and unstable manifolds. Applying Lyapunov's centre theorem, we obtain that there is a family of periodic orbits around each fixed point parametrized by the energy. That is, for each value of the energy, there are two periodic orbits, called the Lyapunov orbits, around the points L_1 and L_2. These periodic orbits are unstable and, therefore, they have two-dimensional stable and unstable invariant manifolds. The invariant manifolds of the Lyapunov orbits are two-dimensional objects in the three-dimensional energy surface; we can think of them as forming tubes in the phase space. These tubes provide the boundaries between orbits that will or will not have a transition between the exterior region, the Jupiter region and the interior region. These tubes form a template of dynamical channels between these regions. This is explained in detail in [3].

2.2. Planar dynamics using a Poincaré section

The mass parameter for the Sun–Jupiter–comet system is $\mu = 0.000\,9537$, which is of course the largest μ amongst the Sun–planet systems. Note that the value $\mu = 0$ corresponds to a system of two bodies: only one primary and the small body. Therefore, the case $\mu = 0$ is equivalent to the (integrable) Kepler problem with one infinitesimal mass. Although one might think at first that the value of μ for the Sun–Jupiter–comet system is numerically small, the system features highly chaotic behaviour. This can be clearly seen from the computation of a Poincaré map. As the Poincaré section, we choose the plane $y = 0$ with $x < 0$, and the map obtained is shown in figure 2.

We observe two types of motion: regular motion in invariant curves forming resonance islands; and chaotic motion scattered around the islands like an 'ocean'. The trajectories lying

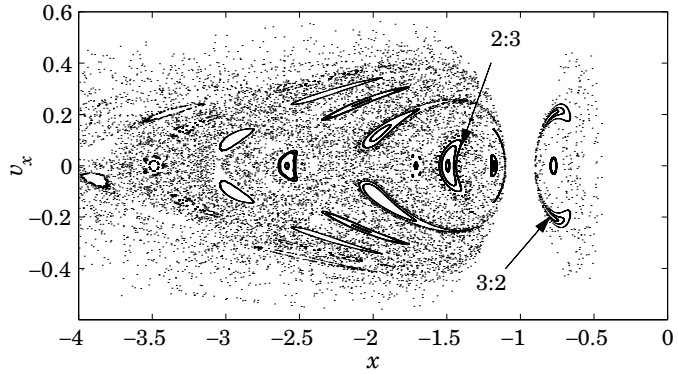

Figure 2. Poincaré section corresponding to $y = 0$, $x < 0$ and energy $E = -1.515$. The arrows indicate the islands of 2:3 and 3:2 resonance with respect to the motion of Jupiter.

on the resonance islands remain in the islands forever; therefore, have constant frequencies. The frequencies nearly satisfy a resonance equation, hence the name of resonance islands. The chaotic trajectories, on the other hand, can visit all the rest of the phase space. As we will see later, some resonance islands influence greatly the dynamics of chaotic trajectories, since they can be trapped around the islands temporarily. Particularly, we will observe closely the island in the interior region in 3:2 resonance with respect to the motion of Jupiter (that is, the trajectories in this island complete three revolutions around the Sun at the same time that Jupiter revolves two times around the Sun); and the island in the exterior region in 2:3 resonance with Jupiter. These two islands are indicated in figure 2.

3. Instantaneous frequency analysis

In this section, we shall define the instantaneous frequency of a system and recall the relevant class of functions for this to be meaningful, the class of asymptotic analytic signals. In the following section, we shall make this more practical and extend its scope by the inclusion of wavelet techniques.

Time–frequency analysis allows us to reproduce the picture of the Poincaré map (figure 2) in terms of the variation in time of the frequencies associated with the trajectories. We will show the capability of time–frequency analysis based on wavelets to discern regular from chaotic motion in the restricted problem. With time–frequency analysis, we can also identify when the motion of the small body is in resonance with respect to the motion of the primaries. We are able to determine exactly when a chaotic trajectory 'visits' a resonant area, by attaining a frequency very close to a resonance for some period of time. We will see that the resonance transitions shed light on the mechanism of transport between the inner and outer regions of the solar system, and reproduce the template that the invariant manifolds of the Lyapunov periodic orbits provide.

The frequency map is traditionally defined in the context of completely integrable Hamiltonian systems; that is, systems for which there is a set of independent integrals of motion which are in involution, and for which the number of integrals is the same as the number of degrees of freedom. If this is the case, it is theoretically possible to find a canonical transformation that allows us to express the Hamiltonian system in action-angle variables in which the frequency map is defined. The significance of the frequency map arises from the

fact that the frequencies associated with such systems completely describe the dynamics. We start this section by recalling the definition of the frequency map, which is the motivation for the numerically computed frequency map that will result from the time–frequency analysis of the trajectories.

3.1. Frequency map

Consider a completely integrable Hamiltonian system with n degrees of freedom expressed in action-angle coordinates,

$$H(I, \theta) = H_0(I);$$

the equations of motion are given by

$$\dot{I}_k = 0, \qquad \dot{\theta}_k = \frac{\partial H_0}{\partial I_k}(I) =: \omega_k(I). \tag{3}$$

Therefore, the solutions can be easily obtained as functions of time,

$$I_k(t) = I_k^0,$$
$$\theta_k(t) = \omega_k(I^0)t + \theta_k^0, \qquad k = 1, \ldots, n.$$

Therefore, the motion takes place on a torus parametrized by the vector I_0.

The frequency map is defined as

$$I \longmapsto \omega(I), \tag{4}$$

and $\omega_1, \omega_2, \ldots, \omega_n$ are said to be the frequencies of the torus with parameters $I_1, I_2, \ldots I_n$. If the frequency map is invertible, we can use the frequencies instead of the actions as the coordinates.

The frequencies completely determine the dynamics on the torus: if the frequencies are non-resonant, that is, if

$$m_1\omega_1 + m_2\omega_2 + \cdots + m_n\omega_n \neq 0$$

for all integer numbers m_k, then the motion is quasiperiodic and all trajectories are dense in the torus. On the other hand, if the equation

$$m_1\omega_1 + m_2\omega_2 + \cdots + m_n\omega_n = 0$$

is satisfied for some integer vector $(m_1, m_2, \ldots, m_n)$, then we say that the torus is resonant and in that case, the trajectories lie in lower dimensional tori, depending on the multiplicity of the resonance.

The definition of the frequency map (4) depends on the representation in action-angle coordinates of the integrable Hamiltonian system. The same definition is used for nearly-integrable systems (that is, when a small perturbation is added to an integrable system). In this case, the KAM theorem [16, 17] guarantees that most tori remain after the perturbation, and so many solutions are quasiperiodic and therefore frequencies can be defined in the traditional way.

The use of action-angle coordinates is possible only locally in most systems, and furthermore, many systems are not integrable or even nearly integrable, and so the previous analysis does not apply, even in principle. Instead, we will proceed numerically.

As a motivation, note that the solutions of (3) can be expressed in complex coordinates as

$$z_k(t) = \sqrt{2I_k^0}\, \mathrm{e}^{\mathrm{i}(\omega_k(I^0)t + \theta_k^0)},$$

and then the frequencies can be extracted from the numerical solutions using Fourier analysis, independent of the form of the Hamiltonian.

With wavelet-based time–frequency analysis we are able to define a frequency map for a much larger class of Hamiltonian systems [1]. We will use the concept of *instantaneous frequency* to extend the frequency map analysis to Hamiltonian systems that are not nearly integrable, or that are not given in action-angle coordinates.

3.2. Instantaneous frequency—a motivating example

We want to use a definition of time-varying frequency that agrees with the intuitive notion of frequency as the 'oscillation rate'. This definition must agree with the usual notion of Fourier frequency for signals with constant amplitude and frequency. In this way, periodic and quasiperiodic functions will retain their frequencies and the frequency map in the new analysis will coincide with the usual definition (4) for completely and nearly integrable Hamiltonian systems.

There are many different ways to define time-varying frequencies (see for instance [18]), some of them having physical inconsistencies [19]. Consider for instance the following example. Assume that a complex function f is represented as a complex exponential with time-varying amplitude and phase,

$$f(t) = A(t)\,\mathrm{e}^{\mathrm{i}\phi(t)}. \tag{5}$$

Our intuition suggests that the frequency is given by the time derivative of the phase:

$$\omega(t) = \frac{1}{2\pi}\phi'(t).$$

(We adopt the convention of the factor 2π in the definition of frequency.) However, the representation (5) is not unique. To illustrate this with a simple example, consider

$$f(t) = A(t)\cos(t),$$

where $A(t)$ is bounded. According to our intuition, f has a constant frequency $1/2\pi$. Let $\tilde{A} = \sup|A(t)|$, and define the new function $\tilde{f}(t) = (1/\tilde{A})f(t)$. Since $|\tilde{f}(t)| \leqslant 1$, there exists $\tilde{\phi}$ such that $\tilde{f}(t) = \cos(\tilde{\phi}(t))$. Therefore,

$$f(t) = \tilde{A}\cos(\tilde{\phi}(t))$$

is another representation of f that yields a different instantaneous frequency $\tilde{\phi}'(t)/2\pi$. We need to define an instantaneous frequency that can be uniquely determined and that corresponds to our physical intuition. The definition that satisfies the previous conditions and is widely used is based on the concept of analytic signal.

3.3. Analytic signals

The most common definition of instantaneous frequency involves the concept of *analytic signal*, introduced originally by Gabor [20] and Ville [21]. This definition agrees with the notion of Fourier frequency for periodic signals.

A function f is called an analytic signal if either of the following three conditions is satisfied:

(i) The Fourier transform $\hat{f}$ of f satisfies

$$\hat{f}(\xi) = 0 \qquad \text{for} \quad \xi < 0.$$

(ii) If we express f in terms of its real and imaginary parts, $f = u + \mathrm{i}v$, then

$$Hu(t) = v(t),$$

where

$$Hu(t) = -\frac{1}{\pi} P \int_{-\infty}^{\infty} \frac{u(\eta)}{\eta - t}\, \mathrm{d}\eta,$$

is the Hilbert transform. P denotes the principal value integral.

(iii) f is the restriction to real time t of a complex function $\Psi(t + \mathrm{i}\tau)$ that is analytic in the upper half complex plane; that is, Ψ is analytic for $\tau \geqslant 0$.

Using contour integrals in the complex plane, it can be shown that these three characterizations of analytic signals are equivalent. This is useful since for analytic functions the real and imaginary parts are uniquely determined, and so is the phase.

3.4. Definition of the instantaneous frequency

For the class of analytic signals, we define the instantaneous phase and frequency in a unique way as follows.

Definition 1. *Let $f = u + \mathrm{i}v$ be an analytic signal, where u and v are the real and imaginary parts, respectively. The* instantaneous amplitude and phase *of f are defined by*

$$A_f(t) = \sqrt{u(t)^2 + v(t)^2}, \qquad \phi_f(t) = \operatorname{Arctan}\frac{v(t)}{u(t)},$$

and the instantaneous frequency *is the time derivative of the phase:*

$$\omega(t) = \frac{1}{2\pi}\phi_f'(t).$$

For an analytic signal, the representation in polar form $f(t) = A_f(t)\,\mathrm{e}^{\mathrm{i}\phi_f(t)}$ is called *canonical* due to the uniqueness of the instantaneous amplitude and phase.

3.5. Identification of analytic signals

We next discuss the applicability of the definition of time-varying frequencies regarding analytic signals. To determine if a given function is an analytic signal is not an easy task. All three possible characterizations given above are hard to use in practice and the analysis must be done numerically in most cases. One way to proceed is to compute the Fourier transform of the function using an FFT algorithm and check if the coefficients corresponding to negative frequencies are zero. Often, the analytic signal is constructed from a real signal by computing the imaginary part using the Hilbert transform.

In general, functions arising from physical signals or solutions of differential equations are not analytic signals; that is, they have singularities when viewed as functions of complex time. Even for simple cases, the definition of an analytic signal cannot be rigorously applied to obtain the frequency. Consider for instance the one-degree-of-freedom pendulum, which is of course integrable and the Hamiltonian is analytic. Therefore, the frequency can be defined as in (4). However, the solutions can be expressed explicitly in terms of the inverse elliptic functions that have a lattice of singularities in the complex plane; i.e., most solutions are not analytic signals.

The result of Forstneric [22] on complex Hamiltonian systems is another example that shows how restricted the definition of analytic signal can be. It is shown that the only Hamiltonian system in $\mathbb{C}^2$ of the form

$$H(z_1, z_2) = \tfrac{1}{2}{z_2}^2 + Q(z_1) \tag{6}$$

for which all solutions are analytic in the entire complex plane, is for Q quadratic. That is, if Q is not a quadratic function, every solution of (6) contains a singularity, i.e. a point that flows to infinity in finite (complex) time.

In practical terms, the restriction of defining instantaneous frequencies only for functions of real time with analytic continuation to the whole upper half plane (i.e. analytic signals) is too strong. However, in many physical systems we find signals that are very close to an analytic signal, and for which we want to assign an instantaneous frequency. Correspondingly, Delprat *et al* [23] introduced the concept of an asymptotic analytic signal.

3.6. Asymptotic analytic signals

Consider the real function $u(t) = A(t)\cos(\phi(t))$, and its associated analytic signal

$$Z_u(t) = u(t) + \mathrm{i}H[u(t)],$$

$u(t)$ is called an *asymptotic analytic signal if* $Z_u(t)$ is close to $A(t)\,\mathrm{e}^{\mathrm{i}\phi(t)}$.

Note that in general $H[A(t)\cos(\phi(t))] \neq A(t)\sin(\phi(t))$. If $u(t) = A(t)\cos(\phi(t))$ is an asymptotic analytic signal, its representation in terms of $A(t)$ and $\phi(t)$ is close to the canonical representation given by the analytic signal; one has

$$A(t) \approx \sqrt{u(t)^2 + H[u(t)]^2} \qquad \text{and} \qquad \phi(t) \approx \operatorname{Arctan}\frac{H[u(t)]}{u(t)}.$$

Using arguments of stationary phase, it can be shown that the function $A(t)\cos(\lambda\phi(t))$ is an asymptotic analytic signal when λ is large [24], that is, when the oscillations due to the term $\cos(\lambda\phi(t))$ are much more important than the variations of the amplitude $A(t)$.

The characterization of asymptotic analytic signals is useful in practice, since very often we deal with signals for which the variation of the amplitude is much slower than the oscillations. Particularly, this is the case of the orbits of the CRTBP.

In the following, we discuss the extraction of the instantaneous frequency using the wavelet transform for the case of analytic signals. This will result in a numerical algorithm that provides an efficient way to assign and compute a time-varying frequency. The same derivation can be made for asymptotic analytic signals, expanding in terms of the parameter λ in $A(t)\exp(\lambda\phi(t))$ and making λ large [24].

4. Instantaneous frequency and the wavelet transform

We have seen above that the definition of instantaneous frequency for analytic signals is hard to apply in practice. Moreover, most oscillatory physical signals are not analytic signals, but are only close to one. In order to define and extract the instantaneous frequency, we will construct an expansion of the signal in terms of basis functions (wavelets) that localize the signal in both frequency and time.

Fourier analysis is widely used to extract the spectral information of signals. This is done by expanding the signal in terms of a basis of complex exponentials with certain frequency; the coefficients of this expansion express the signal in the frequency domain. However, any temporal features of the frequency are not reflected at all in the frequency representation; for this we need the time representation as well as the frequency representation, a time–frequency analysis.

There are mainly two methods to extract the time variation of the frequencies: the *Gabor transform* and the *wavelet transform*. Both methods involve integral transforms, obtained from the expansions in terms of basis functions that depend on two parameters corresponding

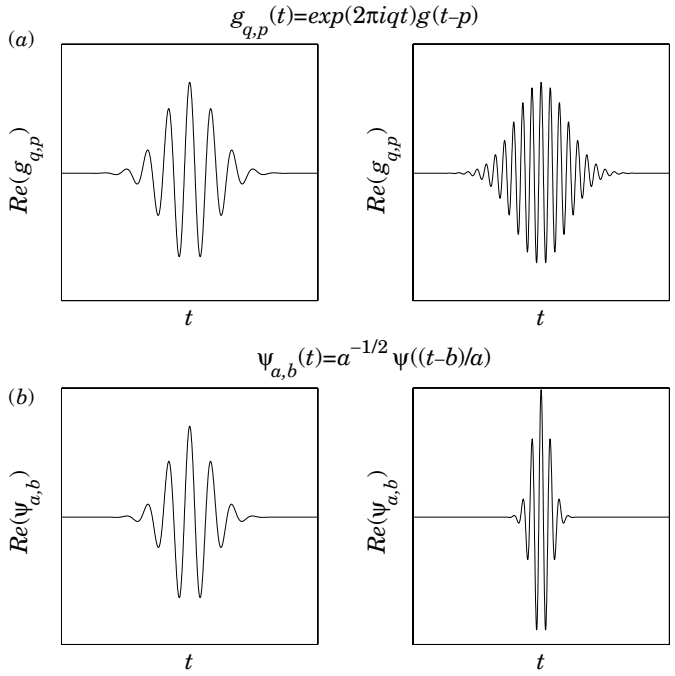

Figure 3. Analysing functions in (*a*) the Gabor transform and (*b*) the wavelet transform. The plots correspond to low frequency on the left and high frequency on the right. Note that for the Gabor transform the envelope remains unchanged; meanwhile in the wavelet transform the envelope is automatically wide for low frequencies and narrow for high frequencies.

to time and frequency. However, they are fundamentally different in the way these basis functions are generated, and have different properties as a result of the definition.

4.1. Gabor transform

To include the time variation in the computation of frequencies, one attempt consists of the introduction of a second parameter in the Fourier transform; this parameter will localize the spectral information around a given point in time. This results in the *Gabor transform* [25, 26] in which the analysing function is the usual complex exponential of the Fourier transform multiplied by an envelope g, a function that acts like a time window:

$$Gf(q, p) = \int_{-\infty}^{\infty} f(t)\, \mathrm{e}^{-2\pi \mathrm{i}\, qt}\, \bar{g}(t - p)\, \mathrm{d}t.$$

The function g is usually a Gaussian but other functions can be used as well. Therefore, the Gabor transform consists of the expansion of the signal in terms of basis functions that involve the complex exponential inside an envelope. The parameter q is the frequency variable, and the parameter p slides the envelope continuously, in that way localizing the signal.

In figure 3(*a*), we represent the analysing or basis functions for two different frequencies. Note that the shape and size of the window remain unchanged for any value of the frequency, therefore it needs to be given *a priori*. Since the size of the time window has to be predetermined, this may produce poor localization and rapid transitions can be missed. Wavelets can overcome this problem.

4.2. Wavelet transform

A good method to analyse functions that have time-varying frequencies is the *wavelet transform* [26]. The wavelet transform provides good localization in both time and frequency, and will allow us to compute instantaneous frequencies of the trajectories. We will see below that there is an interesting relation between the wavelet transform and the instantaneous frequency of an analytic signal. This will allow us to generalize the procedure towards numerical algorithms to extract time-varying frequencies.

The wavelet transform is defined in terms of a function ψ, called the *mother wavelet*, in the following way

$$L_\psi f(a,b) = \frac{1}{\sqrt{a}} \int_{-\infty}^{\infty} f(t) \bar{\psi} \left(\frac{t-b}{a} \right) \mathrm{d}t.$$

To be useful the mother wavelet $\psi \in L^2(\mathbb{R})$ must be like a wave with short duration; i.e., it must have compact support or decay rapidly to 0 for $|t| \to \infty$. There are many wavelets used in the literature, such as the 'mexican hat', Haar and spline wavelets. In our case, we prefer to work with a mother wavelet that has an analytic expression (some wavelets can only be evaluated numerically) and that is a smooth function. Such is the case of the Morlet–Grossman wavelet [25]

$$\psi(t) = \frac{1}{\sigma\sqrt{2\pi}} \, \mathrm{e}^{2\pi \mathrm{i} \lambda t} \, \mathrm{e}^{-t^2/2\sigma^2}.$$

The wavelet transform also depends on two parameters: a is called the scale and is a multiple of the inverse of the frequency; and b is the time parameter that slides the wavelet as a time window. In figure 3(b), we represented the analysing functions (basis functions) of the wavelet transform for different frequencies. Note that the envelope automatically contracts for high frequencies and expands for low frequencies. This is the main advantage of the wavelet transform over the Gabor transform, since this capability of adapting the time window to the frequency range produces better localization in frequency and time.

4.3. Wavelet transform of an analytic signal

The wavelet transform consists of the expansion of a function in terms of wavelets ψ_{ab} that are constructed as dilations and translations of the mother wavelet ψ:

$$\psi_{ab}(t) = \frac{1}{\sqrt{a}} \psi \left(\frac{t-b}{a} \right), \qquad b \in \mathbb{R}, \quad a > 0.$$

We are going to describe how wavelet analysis can be used to extract the instantaneous frequency of an analytic signal. All the arguments follow closely [23] and [25], and are explained here for completeness.

Let $f(t) = A_f(t) \exp[\mathrm{i}\phi_f(t)]$ be an analytic signal. The wavelet transform coefficients are given by

$$L_\psi f(a,b) = \langle f, \psi_{ab} \rangle = \frac{1}{\sqrt{a}} \int_{-\infty}^{\infty} f(t) \bar{\psi} \left(\frac{t-b}{a} \right) \mathrm{d}t.$$

If the wavelet ψ is an analytic signal itself, and if it is written in the form

$$\psi(t) = A_\psi(t) \exp[\mathrm{i}\phi_\psi(t)],$$

then the wavelet transform coefficients can be computed as

$$L_\psi f(a,b) = \frac{1}{\sqrt{a}} \int_{-\infty}^{\infty} M_{ab}(t) \exp[\mathrm{i}\Phi_{ab}(t)] \, \mathrm{d}t, \tag{7}$$

where

$$M_{ab}(t) = A_f(t)A_\psi\left(\frac{t-b}{a}\right),$$
$$\Phi_{ab}(t) = \phi_f(t) - \phi_\psi\left(\frac{t-b}{a}\right).$$

In order to obtain an asymptotic expression for integral (7), we note that if the integrand oscillates greatly due to the term $\exp[\mathrm{i}\Phi_{ab}(t)]$, then the function $M_{ab}(t)$ appears as a constant and the contributions of successive oscillations effectively cancel. However, if the phase $\Phi_{ab}(t)$ is constant this effect is reduced. Therefore, the coefficients of the wavelet transform will 'concentrate' around the critical points of the phase; these points are called *stationary*.

This is a special case of a more general result known as the method of stationary phase [27]. The method computes an asymptotic approximation of the following integral:

$$I = \int_{-\infty}^{\infty} M(t)\exp[\mathrm{i}\lambda\phi(t)]\,\mathrm{d}t.$$

Assuming t_0 is a unique point such that $\phi'(t_0) = 0$, and that $\phi(t_0) \neq 0$ and $\phi''(t_0) \neq 0$ (t_0 is called a non-degenerate stationary point), then

$$I = M(t_0)\exp[\mathrm{i}\lambda\phi(t_0)]\sqrt{\frac{2\pi}{\lambda|\phi''(t_0)|}}\exp[\mathrm{i}\,\mathrm{sgn}(\phi''(t_0))\pi/4] + O(\lambda^{-3/2}).$$

Applying the method of stationary phase to approximate the integral in equation (7), if t_0 is a stationary point, we obtain the expression,

$$L_\psi f(a,b) \approx \frac{1}{\sqrt{a}}f(t_0)\bar{\psi}\left(\frac{t_0-b}{a}\right)\sqrt{\frac{2\pi}{|\Phi''_{ab}(t_0)|}}\,\mathrm{e}^{\mathrm{i}\,\mathrm{sgn}\Phi''_{ab}(t_0)\pi/4}, \tag{8}$$

where $t_0 = t_0(a,b)$. Then the equation $t_0(a,b) = b$ gives a curve in the time-scale plane, and the wavelet transform will concentrate around this curve since it is formed by stationary points. This leads to the following definition.

Definition 2. *The* ridge *of the wavelet transform is defined to be the collection of points for which* $t_0(a,b) = b$.

From the equation $\Phi'_{ab}(t_0) = 0$, we have that

$$\Phi'_{ab}(t_0) = \phi'_f(t_0) - \frac{1}{a}\phi'_\psi\left(\frac{t_0-b}{a}\right) = 0, \tag{9}$$

and then, by definition, the points on the ridge satisfy

$$a =: a_r(b) = \frac{\phi'_\psi(0)}{\phi'_f(b)}.$$

Therefore, the instantaneous frequency $\phi'_f(b)$ of the function f can be obtained from this equation as $\phi'_f(b) = \text{constant}/a_r(b)$ (where b is the time parameter, which we refer to from now on as t) once we have determined the ridge of the wavelet transform.

Although this definition depends on the choice of the wavelet ψ, in practice we find that the ridge of the wavelet transform of a given signal can be computed with several digits of accuracy for both the Morlet–Grossman and the 'mexican hat' wavelets.

4.4. Computation of the ridge of the wavelet transform

The ridge can be obtained from the modulus of the wavelet transform, by computing the maximum modulus (with respect to scale) for each point in time. For a more detailed description of the numerical algorithm for this approach, we refer the reader to [1]. Delprat *et al* [23] described an algorithm to extract the ridges from the phase of the wavelet transform of f. This procedure is described in the appendix.

In this work, we use the Morlet–Grossman wavelet [25],

$$\psi(t) = \frac{1}{\sigma\sqrt{2\pi}}\, \mathrm{e}^{2\pi \mathrm{i}\lambda t}\, \mathrm{e}^{-t^2/2\sigma^2},$$

where σ and λ are parameters that can be tuned to obtain better resolution. For our case, $\sigma = 1$ and $\lambda = 0.8$ proved to be convenient to detect rapid transitions in the frequency. The main features of the computations can be reproduced with the 'mexican hat' wavelet, a real valued wavelet. However, the numerical algorithm is more stable when the Morlet–Grossman wavelet (complex valued) was used.

It is easy to notice the resemblance between the Morlet–Grossman wavelet and the basis functions of the Gabor transform described above. However, one should not forget that for the wavelet transform the basis functions are generated as wavelets having the capability to adapt according to the value of the frequency involved. The time window of the Gabor transform will not adapt, the same envelope will be used for all ranges of frequencies.

The computation of the instantaneous frequency of a signal f can be achieved with the following procedure:

(i) For a point in time $t = b_i$, we obtain an initial approximation of the instantaneous frequency by computing the scale a^0 that produces the maximum modulus of the wavelet transform of f among a suitable set of test scales. This produces the initial approximation to the frequency as constant$/a^0$.

(ii) The scale a^0 is the initial approximation for the algorithm described in the appendix. This procedure will generate a sequence of points that converge to the scale a^* that corresponds to the instantaneous frequency at $t = b_i$: $\omega(b_i) = \text{constant}/a^*$.

(iii) The value of the frequency at $t = b_i$ can be used as the initial approximation for the frequency at $t = b_{i+1}$.

5. Time–frequency analysis of the CRTBP

We now define a frequency map in the CRTBP based on the computation of instantaneous frequencies of the solutions. This section and the following one describe the treatment of the planar version of the problem, a system of two degrees of freedom. In section 7, we show the results for the spatial problem, and the relation with the planar dynamics.

The frequencies in the planar CRTBP that we shall determine are associated with the representation of the orbits in configuration space in the inertial frame. This choice allows us to compare the frequencies with the frequency of Jupiter and in this way to detect when the comet is in resonance with the motion of Jupiter. Remember that in this frame, Jupiter moves in a circular orbit with (constant) frequency of $1/2\pi$.

In the inertial frame, the orbits in configuration space (X, Y) consist of trajectories winding around the centre of mass of Sun and Jupiter, both in the interior and exterior regions (see figure 1) and in some cases exchanging between them. Sometimes the trajectories are captured in the Jupiter region, meaning that they travel along with Jupiter before they go to a different region.

Although there is no mathematical reason for these orbits to satisfy the definition of the analytic signal, we observe that their Fourier coefficients (as calculated numerically) are relatively small for negative frequencies and hence they are close to an analytic signal. Furthermore, the oscillations of the orbits around the centre of mass are more important than the variation of the amplitude of the orbit, as happens with many oscillatory signals found in physical systems. We are going to treat these orbits as asymptotic analytic signals (see section 3), and extract the instantaneous frequency from their wavelet transform, according to the procedure described in section 4.

The objective is to construct numerically a *frequency map*, by associating the initial condition with the computed time-varying frequency of the corresponding trajectory integrated over a fixed time interval $[0, T]$.

5.1. Frequency map

We have computed the frequency map for numerically generated solutions of the CRTBP (equations (1)) with a particular, chosen energy using the following procedure:

- Initial conditions are taken in the rotating frame coordinates (x, v_x, y, v_y) with a fixed value of the energy of $E = -1.515$. (This is the energy of the comet Oterma.) We pick the initial conditions on an evenly spaced grid in the plane (x, v_x) corresponding to $y = 0, x < -1$; and $v_y > 0$ is chosen to fit the energy level. In this way, we analyse orbits similar to the trajectory of the comet Oterma in the exterior region (see figure 1) before it was captured by Jupiter.
- For each initial condition $\left(x^0, v_x^0\right)$, we numerically integrate the equations of motion to obtain the trajectory $(x, y, v_x, v_y)(t), t \in [0, T]$, for $T = 2000 \approx 318$ Jupiter years. In fact, if we integrate equations (1) directly, trajectories passing near Jupiter usually explode. We need to work with regularized equations that eliminate the singularity caused by collision with Jupiter. We applied the Kustaanheimo–Stiefel canonical regularization in the planar version (two degrees of freedom) and spatial version (three degrees of freedom). We refer the reader to Szebehely [15] (p 582) for more details. We then express the orbit in configuration space in inertial coordinates,
$$f(t) = (X + \mathrm{i}Y)(t) = \mathrm{e}^{-\mathrm{i}t}(x + \mathrm{i}y)(t).$$
- We extract the instantaneous frequency $\omega(t)$ of $f(t), t \in [0, T]$, by computing the ridge of the wavelet transform of $f(t)$. (See section 4.)

  The *frequency map* is expressed as
$$\left(x^0, v_x^0\right) \longmapsto \omega(t), \qquad t \in [0, T].$$

The variation in time of the frequency is a good indicator of whether a trajectory is regular or not. A trajectory with regular motion has a frequency that is constant in time. If the frequency varies in time, this suggests that the orbit is chaotic.

If for a particular initial condition the frequency is constant in time, then the mean frequency $\tilde{\omega}$ is equal to this constant value and coincides with the basic Fourier frequency of the orbit. For chaotic orbits, the mean frequency $\tilde{\omega}$ does not have a physical meaning, but it can be used as reference to compute how much the frequency is varying in time. We consider the average variation of the frequency with respect to $\tilde{\omega}$ as an indicator of how chaotic the trajectory is. We call this average variation the *diffusion*.

The diffusion associated with a trajectory with initial conditions $\left(x^0, v_x^0\right)$ is defined as
$$\text{diffusion} = \frac{1}{T}\int_0^T |\omega(t) - \tilde{\omega}|\,\mathrm{d}t. \tag{10}$$

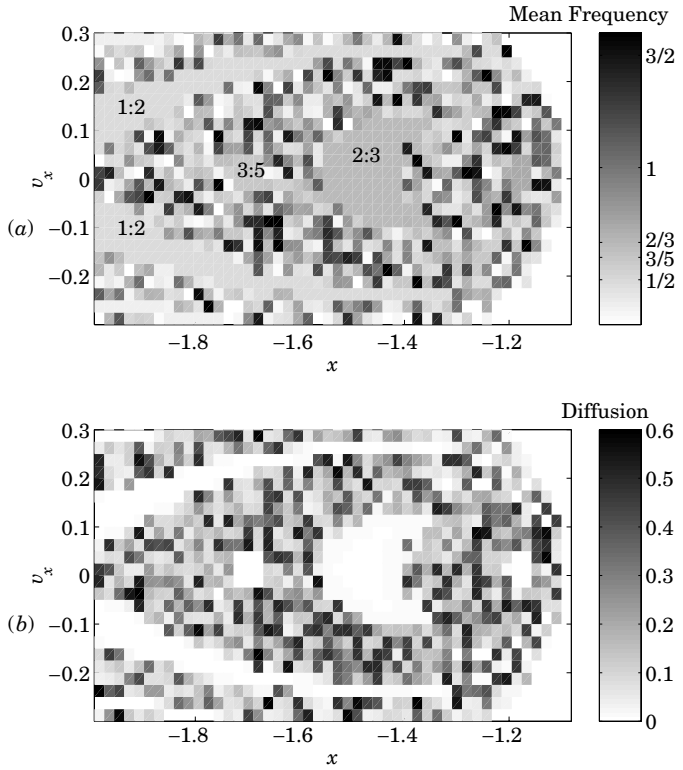

Figure 4. Phase space structure from time–frequency analysis: (*a*) the mean frequency (divided by the frequency of Jupiter) and (*b*) the diffusion plot. See the text for more details.

6. Results

The frequency map is summarized in figure 4. In (*a*), we present the density plot of the mean frequencies $\tilde{\omega}$ on the plane of initial conditions (x, v_x). The shades of grey represent the mean frequency divided by the frequency of Jupiter; that is, a mean frequency of 1 represents a trajectory which has the same frequency as Jupiter. In (*b*), the diffusion obtained with the formula in equation (10) is represented in a similar way.

We see the resemblance between the Poincaré map (figure 2) and the density plots of the mean frequency and diffusion (figure 4). The regions corresponding to chaotic trajectories have a significant mixture of frequencies, and high values of diffusion. We can also easily identify in figure 4 regions for which the trajectories have the same frequency and low diffusion, and see that they correspond to resonance islands. In particular, we detect the 2:3, 1:2 and 3:5 resonances.

6.1. Results for individual trajectories

With time–frequency analysis we can also analyse individual trajectories. In figure 5, we present two trajectories with interesting dynamics: they have large diffusion but remain close to a resonance for some time. The orbit in the inertial coordinates is plotted in the first panel, and the time-varying frequency divided by the frequency of Jupiter is represented in the second panel. The lines labelled 2:3 and 3:2 were plotted as a reference; they correspond to the value of frequency that is in such resonance with the motion of Jupiter.

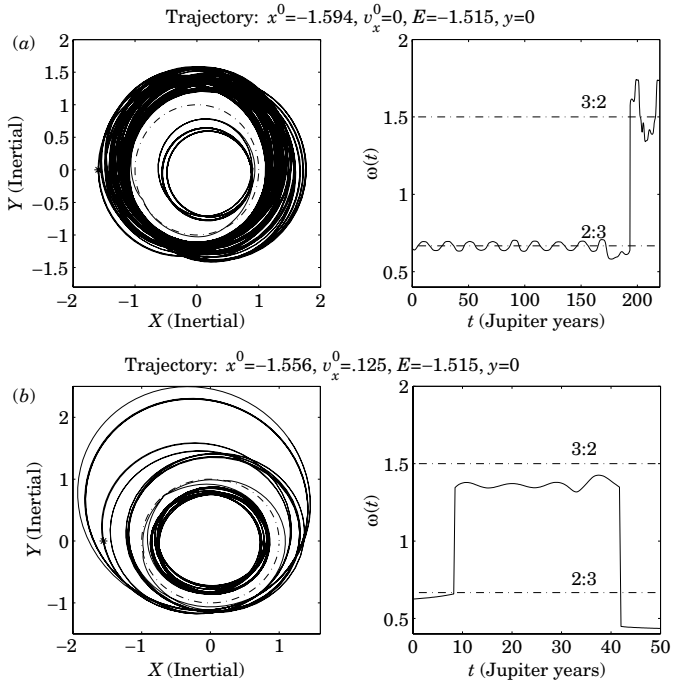

Figure 5. Examples of trajectories and their frequency evolution. The orbits are represented in the inertial frame and the dotted line is the orbit of Jupiter. The time-varying frequency is divided by the frequency of Jupiter. Note that the trajectories that go from the exterior region to the interior region 'visit' some resonances.

Figure 5(*a*) displays a chaotic trajectory with frequency close to the 2:3 resonance; it remains there for a long time before it drifts away. In figure 5(*b*), we see a trajectory that jumps from near the 2:3 resonance to near the 3:2 resonance, and jumps again to the 1:2 resonance.

The time-varying frequency reflects accurately the behaviour of the solution. Recall that the initial conditions were taken with $y = 0$ and $x < -1$ in the exterior region, on the side opposite to Jupiter (see figure 1). The trajectory in figure 5(*a*) corresponds to an initial condition close to the island of 2:3 resonance in the exterior region, that is 'trapped' around the island for some time, behaving almost regularly (as we can see in the plot of the orbit in inertial coordinates), until some point in time when the trajectory is 'released' from the resonance. This trajectory features a *resonance trapping* that we can detect by observing the evolution of the frequency in time.

In the same way, we are able to determine *resonance transitions*. The trajectory in figure 5(*b*) corresponds to an orbit that evolves from the exterior region, close to the island of 2:3 resonance, to the interior region, passing near the island of 3:2 resonance; and then to the exterior region going towards the 1:2 resonance.

6.2. Resonance trappings, resonance transitions and transport

We found that many trajectories that evolve from the exterior region to the interior region also feature a resonance transition between the 2:3 and 3:2 resonances. This in fact can be seen

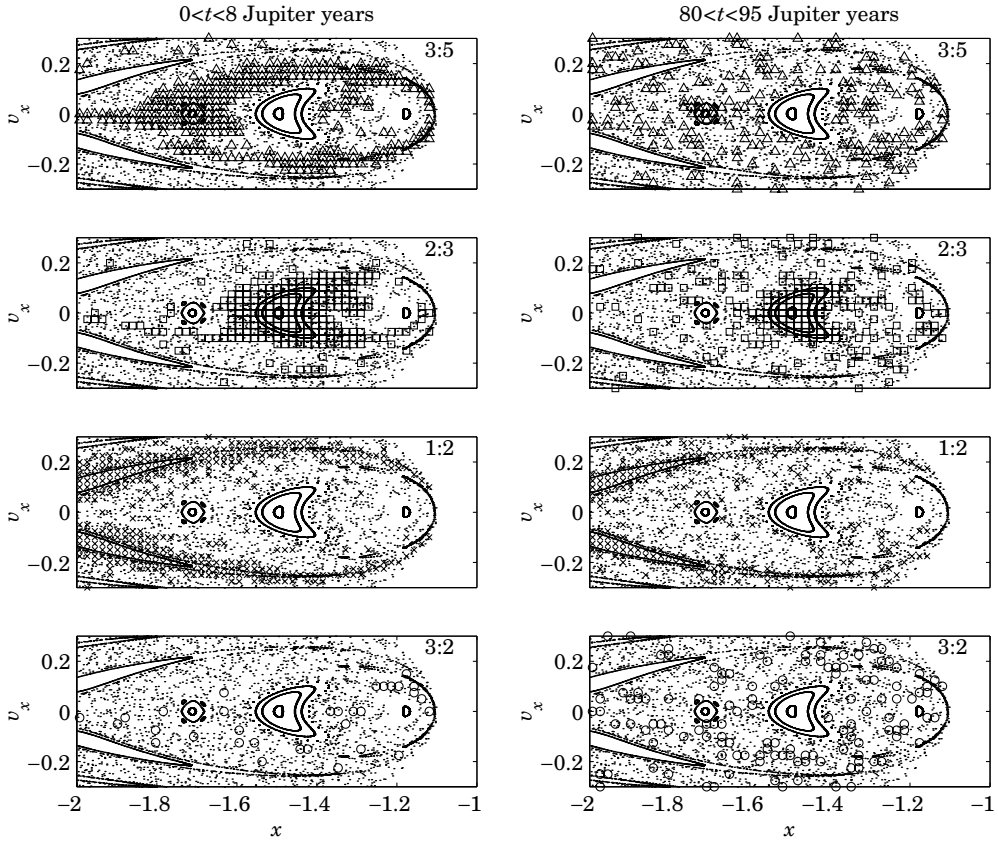

Figure 6. Temporary resonance trappings. We show the initial conditions of orbits that during the time interval indicated were captured for at least 1 Jupiter year in a given resonance. Since the 3:2 resonance is in the interior region around the Sun, trapping in this resonance means that the trajectory has exchanged from the exterior region to the interior region.

as an implication of the transport mechanism between the exterior and interior regions of the solar system.

Therefore, by looking at the evolution of the frequency, we can determine which trajectories exchanged from the exterior region across the Jupiter region continue evolving in the interior region, or vice versa. Since time–frequency analysis yields the precise time at which a resonance transition happens, we can determine how trajectories are being transported in different regions of the phase space.

These transitions are represented in figure 6. We marked the initial conditions corresponding to trajectories that have undergone a resonance trapping on a given interval of time. The Poincaré map is in the background for reference. The left column corresponds to the beginning of evolution, $0 < t < 8$ Jupiter years. As we can expect, trapped trajectories lie in and around the resonance islands. The right column shows the resonance trappings that occurred during the time interval $80 < t < 95$ (Jupiter years). Naturally the trajectories in the resonance islands are trapped (forever), but many chaotic trajectories keep having temporary resonance trappings during all of the evolution. Note that if an initial condition is marked in different plots, it means that a resonance transition has occurred during that time interval. We

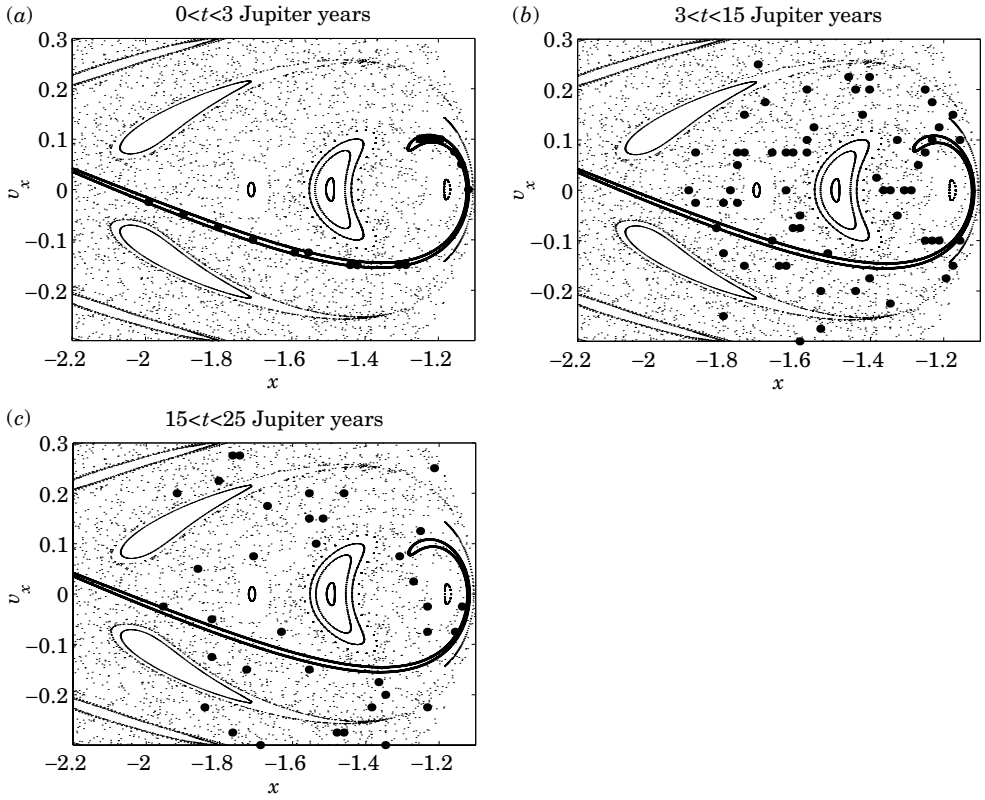

Figure 7. The large dots represent initial conditions of orbits that feature rapid transition from the exterior to the interior regions, during the time interval indicated. The thick curve represents the first backward intersection of the stable manifold of the Lyapunov orbit around L_2 with the Poincaré section, which is a closed curve; all trajectories that have a transition to the interior region in less than 3 Jupiter years are inside this curve. The dots in the background correspond to the Poincaré map.

can also observe that, up to this time, many trajectories keep exchanging between the exterior and interior regions and vice versa.

6.3. Rapid transitions

Transitions between the exterior region and the interior region occur when there is a sudden change in frequency, from a frequency less than Jupiter's frequency, to one that is greater than Jupiter's. We used the frequency map to detect these transitions: if at a given point in time there is a change in the relative frequency with respect to the frequency of Jupiter from less than 1 to greater than 1, then a transition has taken place.

The rapid transitions were detected and represented in figure 7. Large dots represent the initial conditions corresponding to trajectories that have a transition between the exterior region and the interior region during three different intervals of time. The background dots represent the Poincaré map for reference.

Koon *et al* [3] have shown that the stable manifold of the Lyapunov orbit around L_2 serves as a dynamical channel for capturing orbits: all trajectories that go from the exterior region

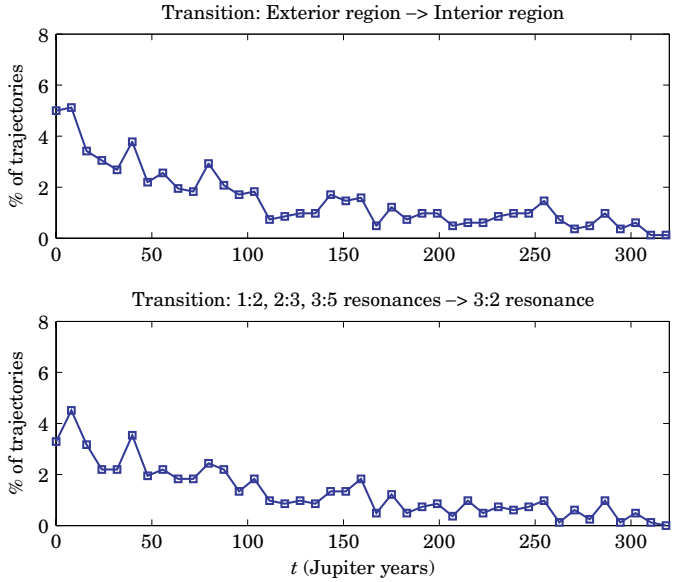

Figure 8. Percentage of trajectories that for the first time have a transition from the exterior region to the interior region, as a function of time; and similarly from the outer resonances (2:3, 1:2 and 3:5) to the inner resonance 3:2.

to the Jupiter region must be in the interior of the tube formed by this manifold. The first intersection of this manifold in backward time with the Poincaré section $y = 0, x < 0$ is a closed curve (shown in figure 7 as a thick curve). This curve is the boundary of the region of orbits that are going to be captured rapidly into the Jupiter region. Not all orbits captured in the Jupiter region proceed to the interior region; some trajectories can swing around Jupiter and leave towards the exterior region again. Our results agree with the results in [3], since all transitions that happen within 3 Jupiter years (before completing one revolution around the centre of mass) have initial conditions in the interior of this curve, as we can see in figure 7(*a*).

We can observe in parts (*b*) and (*c*) of figure 7 that the distribution of transitions in the time intervals $3 < t < 15$ and $15 < t < 25$ (Jupiter years) is quite irregular. If we wanted to use the method of invariant manifolds to obtain all the trajectories that will get captured in the Jupiter region after a number of revolutions in the exterior region, we would need to find the successive intersections of the stable manifold of the Lyapunov orbit around L_2 in backward time with the Poincaré section. This is computationally very hard due to the extremely complicated dynamics. For instance, intersections of the stable and unstable manifolds of the Lyapunov orbit around L_2 produce foldings and swirls of the manifolds. And there is an intrinsic difficulty in the computation of such invariant manifolds for long time.

6.4. Number of transitions versus time

Figure 8 displays the percentage of trajectories that experience a transition from the exterior to the interior region at a given time. We only considered the first transition of the orbit; therefore each trajectory is counted only once, although it might evolve back and forth between the two regions afterwards. For this calculation, we divided the total evolution time into subintervals of 8 Jupiter years, and counted how many first transitions occurred in each subinterval. The

percentage was calculated with respect to the total number of chaotic trajectories; that is, trajectories in the resonance islands (that remain there for all time) were not considered.

For comparison, the second panel shows the percentage of trajectories that feature a first transition from one of the exterior resonances (2:3, 1:2 and 3:5) to the interior resonance 3:2, as a function of time. Note that the two curves show the same tendency as time grows. Therefore, resonance transitions represent a clear indicator of transport between the two regions.

The decreasing trend of the plots yields a qualitative description of how transitions between the exterior and interior regions take place. If a comet happens to be in the distribution of our initial conditions, and it features a transition, then it is more likely that the comet will exchange towards the interior region within a few Jupiter years; it is very unlikely that the comet will stay in the exterior region for more than 300 Jupiter years and then go to the interior region.

7. Spatial dynamics

The methodology described for the planar CRTBP can naturally be extended to the spatial (three-dimensional) problem; that is, when we let z, v_z into the dynamics. The dimension of the energy surface is now 5. We considered two different slices of the phase space. The first slice was the plane x, v_x with $y = 0$, $z = 0.05$, $v_z = 0$ and $E = -1.515$. This corresponds to a plane just parallel to the one used for the planar case (sections 5 and 6). The second slice corresponds to the plane x, z with $y = 0$, $v_x = 0$, $v_z = 0$ and $E = -1.515$; v_y is chosen to fit the energy level.

In order to define a frequency map, we express the orbits as two signals:

$$f_1(t) = (X + \mathrm{i}Y)(t) = \mathrm{e}^{-\mathrm{i}t}(x + \mathrm{i}y)(t)$$

$$f_2(t) = Z(t) + \mathrm{i}H[Z(t)] = z(t) + \mathrm{i}H[z(t)],$$

where H represents the Hilbert transform (see section 3). We then extract the associated instantaneous frequencies $\omega_1(t)$ and $\omega_2(t)$. We can compute the mean frequencies associated with each initial condition and the diffusion will be computed as the sum of the average deviations for each frequency.

We found that the frequencies ω_1 and ω_2 are practically identical; that is, the motion in the z coordinate is oscillatory and completely driven by the motion in the x, y plane.

Similarly to the planar case, we found some regions of regular motion (close to zero diffusion) surrounded by chaotic regions (high diffusion). In the regular regions, we identified areas that have frequencies in resonance with the frequency of Jupiter, as in the planar case we can clearly distinguish the 2:3, 1:2 and 3:5 resonances, these are shown in figure 9. These regions can be interpreted as the higher dimensional analogue of the islands found in Poincaré maps of systems with two degrees of freedom. We also observed that for orbits starting with $|z^0| > 0.1$, the total diffusion is small; that is, orbits with large z remain in the exterior region and have slow variation in frequency.

In figure 9, we also show with large dots the initial conditions of trajectories that have a transition from the exterior region to the interior region. In (*a*), we show the initial conditions of rapid transitions, within 3 Jupiter years (these are orbits that start with $z^0 = 0.05$). They are in a region similar to the corresponding one in the planar case $z^0 = 0$ (in figure 7(*a*)). This corresponds to a generalization to three degrees of freedom of the critical region that Koon *et al* [3] found for the planar case: there is a region in which all orbits will enter the Jupiter region and possibly go to the interior region. In (*b*), the large dots correspond to transitions that happen within 20 Jupiter years. Note that only orbits close to the x, y plane ($z^0 < 0.1$) have the chance to enter the interior region.

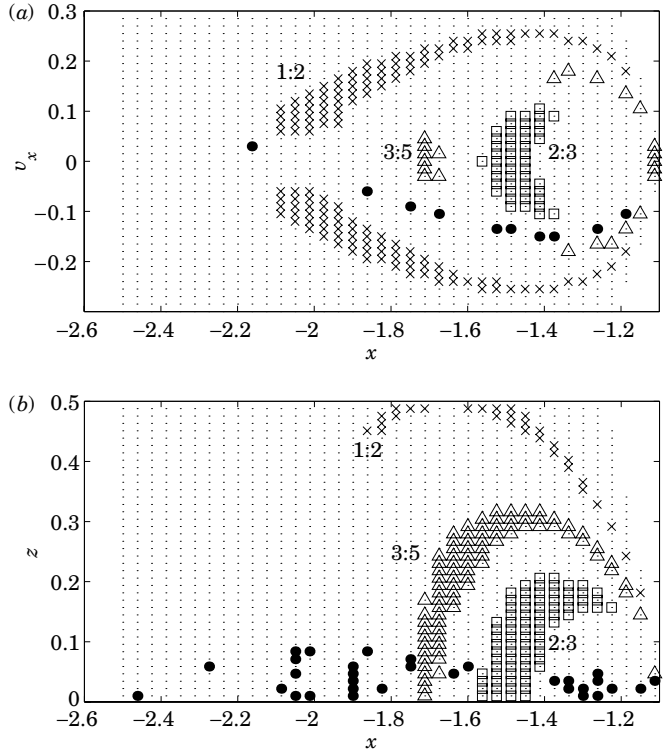

Figure 9. Resonant regions in the spatial problem, and some transitions to the interior region. The initial conditions studied (small dots) were in two slices: (*a*) the first slice is in the x, v_x plane, with $y = v_z = 0, z = 0.05, E = -1.515$ and (*b*) the second slice is in the x, z plane: $y = 0$, $v_x = 0$, $v_z = 0$ and $E = -1.515$. The large dots represent transitions to the interior region, in (*a*) the transitions happened in less than 3 Jupiter years (compare with figure 7(*a*) for the planar case), and in (*b*) they happen within 20 Jupiter years.

8. Conclusions

This paper has presented the method of time–frequency analysis based on wavelets, and showed that it provides a powerful tool to extract key features of a dynamical system from its numerical solutions. The technique was illustrated using both the planar and the spatial versions of the circular restricted three-body problem. Based on the variation in time of the frequencies calculated from the wavelet transform, the method can distinguish regular trajectories (corresponding to resonant islands) from chaotic ones. We are able to determine if a chaotic trajectory has been trapped in a resonance, or if it is undergoing a resonant transition.

The method of time–frequency analysis allows one to detect resonance islands that greatly affect the dynamics. For the CRTBP, transport in the phase space between different regions was resolved by determining resonance transitions of chaotic trajectories. This was achieved by extracting time-varying frequencies of the orbits in configuration space in the inertial frame.

Our results find the same regions that Koon *et al* [3] use in describing the transport mechanism between the exterior and interior regions of the solar system and its relation with resonance transitions. However, since our method includes the time variable in the analysis, we are able to determine exactly when resonance transitions take place, and their distribution along the evolution of the system.

We showed that the resonance transitions between three exterior resonances 2:3, 1:2 and 3:5, and the interior resonance 3:2, reflect a great deal of the transitions between the exterior region and the interior region. We also showed that for energy levels close to the energy of comet Oterma, phase space transport can, to a large extent, be explained using the planar model, since the results in the spatial problem showed that the transitions between different regions only happen for $|z|$ small. We were also able to obtain a region where rapid transitions occur and a description of the resonance trappings, which is something seldom done for a system of three degrees of freedom.

Although the meaning of these results is limited by the finite number of trajectories studied and by the bounded time interval that was used for the frequency map, we have shown the strong relation between transport in phase space and resonance transitions. In the future, we plan to study the effect of longer integration times, for which the use of symplectic or variational integrators is needed to preserve the basic physics of the trajectories and, hence, of the frequencies. We believe that this work will open a course of research in many high-dimensional problems for which the transport mechanism is still to be understood.

Acknowledgments

The research of LVV-A was partially supported by CONACYT Mexico and by the J Ford Fellowship, GaTech. The research of JEM was partially supported by NSF grant DMS-0204474 and by a Max Planck Research Award.

Appendix. Extraction of the ridge of the wavelet transform

Define the phase of the wavelet transform of f (7) as

$$\Psi(a,b) = \mathrm{Arg}(L_\psi f(a,b)).$$

From the asymptotic approximation in equation (8), we obtain

$$\Psi(a,b) \approx \Phi_{ab}(t_0) \pm \frac{\pi}{4}.$$

Note that, from the definition of the ridge of the wavelet transform, $t_0 = t_0(a,b)$, $\Phi_{ab}(t_0)$ is a function of the variables a and b. Then, computing the partial derivative with respect to b we have

$$\begin{aligned}
\frac{\partial \Psi}{\partial b} &\approx \frac{\partial \Phi_{ab}}{\partial b} \\
&= \frac{\partial}{\partial b}\left\{\phi_f(t_0(a,b)) - \phi_\psi\left(\frac{t_0(a,b)-b}{a}\right)\right\} \\
&= \phi_f'(t_0)\frac{\partial t_0}{\partial b} - \phi_\psi'\left(\frac{t_0-b}{a}\right)\left(\frac{\frac{\partial t_0}{\partial b}-1}{a}\right) \\
&= \left[\phi_f'(t_0) - \frac{1}{a}\phi_\psi'\left(\frac{t_0-b}{a}\right)\right]\frac{\partial t_0}{\partial b} + \frac{1}{a}\phi_\psi'\left(\frac{t_0-b}{a}\right) \\
&= \frac{1}{a}\phi_\psi'\left(\frac{t_0-b}{a}\right).
\end{aligned}$$

(In the last step, the quantity in brackets is equal to zero due to equation (9).)

Evaluating at $b = b_0$ (and then $t_0(a,b_0) = b_0$) we obtain

$$\left.\frac{\partial \Psi}{\partial b}\right|_{b=b_0} \approx \frac{1}{a}\phi_\psi'\left(\frac{t_0-b_0}{a}\right) = \frac{1}{a}\phi_\psi'(0).$$

This equation provides an algorithm to extract the scale $a_r(b_0)$ that solves the ridge equation $t_0(a_r(b_0), b_0) = b_0$, for each time value b_0. The algorithm consists of finding the fixed point a that solves the equation

$$a = \frac{\phi'_\psi(0)}{\partial_b \Psi(a, b)},$$

for each b fixed. Therefore, given an initial approximation a^0, we can produce a sequence of points $a^{j+1} = \frac{\phi'_\psi(0)}{\partial_b \Psi(a^j, b)}$ that converges to the solution a^*.

References

[1] Vela-Arevalo L V and Wiggins S 2001 Time-frequency analysis of classical trajectories of polyatomic molecules *Int. J. Bifurcation Chaos* **11** 1359–80

[2] Tsiganis K, Varvoglis H and Hadjidemetriou J D 2000 Stable chaos in the 12:7 mean motion resonance and its relation to the stickiness effect *Icarus* **146** 240–52

[3] Koon W S, Lo M W, Marsden J E and Ross S D 2000 Heteroclinic connections between periodic orbits and resonance transitions in celestial mechanics *Chaos* **10** 427–69

[4] Ross S D, Koon W S, Lo M W and Marsden J E 2003 Design of a multi-moon orbiter *AAS* 03-143

[5] Dellnitz M, Junge O, Koon W-S, Lekien F, Lo M W, Marsden J E, Padberg K, Preis R, Ross S D and Thiere B 2003 Transport in dynamical astronomy and multibody problems *Preprint*

[6] Lichtenberg A J and Lieberman M A 1983 *Regular and Chaotic Dynamics* (New York: Springer)

[7] Contopoulos G and Voglis N 1997 A fast method for distinguishing between ordered and chaotic orbits *Astron. Astrophys.* **317** 73–81

[8] Froeschlé C and Lega E 1998 Twist angles: a method for distinguishing islands, tori and weak chaotic orbits. Comparison with other methods of analysis *Astron. Astrophys.* **334** 355–62

[9] Laskar J, Froeschlé C and Celletti A 1992 The measure of chaos by the numerical analysis of the fundamental frequencies. Application to the standard mapping *Physica* D **56** 253–69

[10] Laskar J 1993 Frequency analysis for multi-dimensional systems. Global dynamics and diffusion *Physica* D **67** 257–81

[11] Binney J and Spergel D 1982 Spectral stellar dynamics *Astrophys. J.* **251** 308–21

[12] Martens C and Ezra G 1987 Classical and semiclassical mechanics of strongly resonant systems—a Fourier transform approach *J. Chem. Phys.* **86** 279–307

[13] Laskar J 1990 The chaotic motion of the solar system: a numerical estimate of the size of the chaotic zones *Icarus* **88** 226–91

[14] Losada J C, Estebaranz J M and Benito R M 1998 Local frequency analysis and the structure of classical phase space of the LiNC/LiCN molecular system *J. Chem. Phys.* **108** 63–71

[15] Szebehely V 1967 *Theory of Orbits* (New York: Academic)

[16] Arnold V I 1963 Proof of a theorem by A N Kolmogorov on the persistence of quasiperiodic motions under small perturbations of the Hamiltonian *Russ. Math. Surv.* **18** 9–36

[17] Arnold V I 1963 Small denominators and problems of stability of motion in classical and celestial mechanics *Russ. Math. Surv.* **18** 85–191

[18] Vakman D 1996 On the analytic signal, the Teager–Kaiser energy algorithm, and other methods for defining amplitude and frequency *IEEE Trans. Signal Process.* **44** 791–7

[19] Mandel L 1974 Interpretation of instantaneous frequency *Am. J. Phys.* **42** 840–6

[20] Gabor D 1946 Theory of communications *J. IEE* **93** 429–57

[21] Ville J 1948 Théorie et applications de la notion de signal analytique *Cables Transm.* **2** 61–74

[22] Forstneric F 1996 Actions of $(\mathbb{R}, +)$ and $(\mathbb{C}, +)$ on complex manifolds *Math. Z.* **223** 123–53

[23] Delprat N, Escudié B, Guillemain P, Kronland-Martinet R, Thamitchian P and Torrésani B 1992 Asymptotic wavelet and Gabor analysis: extraction of instantaneous frequencies *IEEE Trans. Inf. Theory* **38** 644–64

[24] Vela-Arevalo L V 2002 Time-frequency analysis based on wavelets for Hamiltonian systems *PhD Thesis* California Institute of Technology

[25] Carmona R, Hwang W and Torrésani B 1998 *Practical Time-Frequency Analysis: Gabor and Wavelet Transforms with an Implementation in S* (San Diego, CA: Academic)

[26] Daubechies I 1992 *Ten Lectures on Wavelets* (Philadelphia, PA: SIAM)

[27] Copson E T 1965 *Asymptotic Expansions* (Cambridge: Cambridge University Press)